AMERICAN JOURNAL OF PHYSIOLOGY
ENDOCRINOLOGY AND METABOLISM.

Am J Physiol Endocrinol Metab 323: E215–E230, 2022.
First published July 6, 2022; doi:10.1152/ajpendo.00026.2022

RESEARCH ARTICLE

Chronicity in Metabolism

Acute binge alcohol alters whole body metabolism and the time-dependent expression of skeletal muscle-specific metabolic markers for multiple days in mice

Abigail L. Tice,[1] Joseph A. Laudato,[1] Debra A. Fadool,[2] Bradley S. Gordon,[1,3] and Jennifer L. Steiner[1,3]
[1]*Department of Nutrition and Integrative Physiology, Florida State University, Tallahassee, Florida;* [2]*Department of Biological Science, Program in Neuroscience, and Institute of Molecular Biophysics, Florida State University, Tallahassee, Florida; and* [3]*Institute of Sports Sciences and Medicine, Florida State University, Tallahassee, Florida*

Abstract

Alcohol is a myotoxin that disrupts skeletal muscle function and metabolism, but specific metabolic alternations following a binge and the time course of recovery remain undefined. The purpose of this work was to determine the metabolic response to binge alcohol, the role of corticosterone in this response, and whether nutrient availability mediates the response. Female mice received saline (control) or alcohol (EtOH) (5 g/kg) via intraperitoneal injection at the start of the dark cycle. Whole body metabolism was assessed for 5 days. In a separate cohort, gastrocnemius muscles and liver were collected every 4 h for 48 h following intoxication. Metyrapone was administered before alcohol and gastrocnemius was collected 4 h later. Lastly, alcohol-treated mice were compared with fed or fasted controls. Alcohol disrupted whole body metabolism for multiple days. Alcohol altered the expression of genes and proteins in the gastrocnemius related to the promotion of fat oxidation (*Pparα, Pparδ/β,* AMPK, and *Cd36*) and protein breakdown (*Murf1, Klf15, Bcat2*). Changes to select metabolic genes in the liver did not parallel those in skeletal muscle. An alcohol-induced increase in circulating corticosterone was responsible for the initial change in protein breakdown factors but not the induction of *FoxO1, Cebpβ, Pparα,* and *FoxO3*. Alcohol led to a similar, but distinct metabolic response when compared with fasting animals. Overall, these data show that an acute alcohol binge rapidly disrupts macronutrient metabolism including sustained disruption to the metabolic gene signature of skeletal muscle in a manner similar to fasting at some time points.

NEW & NOTEWORTHY Herein, we demonstrate that acute alcohol intoxication immediately alters whole body metabolism coinciding with rapid changes in the skeletal muscle macronutrient gene signature for at least 48 h postbinge and that this response diverges from hepatic effects and those of a fasted animal.

alcohol; ethanol; metabolism; skeletal muscle

INTRODUCTION

Binge drinking is a popular behavior with 17% of adults in the United States reporting an average of ~53 binges a year with ~7 drinks per binge (1, 2). Binge drinking is defined as raising the blood alcohol concentration (BAC) to at least 0.08 g/dL in under 2 h, but higher levels are often achieved (3). This level of alcohol intoxication alters the normal functioning of many organ systems, including the skeletal muscle (4), which is central to metabolic function, movement, and overall health (5). More specifically, skeletal muscle contributes to metabolic homeostasis as it serves as a glucose sink, is the major storage site for amino acids, and participates in fatty acid oxidation (5–8). Metabolic homeostasis is crucial for health. Long-term perturbations to metabolic functioning can lead to a variety of diseases, including metabolic syndrome and diabetes (9).

Alcohol use, including binge alcohol intoxication, alters tissue metabolism as well as substrate utilization and generation throughout the body. For instance, it is known that alcohol can lead to the inhibition of glucose utilization, induction of transient insulin resistance, and suppression of glycogen synthesis (10). Moreover, fat metabolism is modified by acute alcohol intake as low concentrations of alcohol consumed with a high-fat meal promote postprandial lipemia (11), whereas higher concentrations or chronic abuse of alcohol can result in episodes of alcoholic ketoacidosis (12). However, corresponding molecular changes within the

Correspondence: J. L. Steiner (jsteiner2@fsu.edu).
Submitted 1 February 2022 / Revised 22 June 2022 / Accepted 27 June 2022

skeletal muscle during what is termed "the hangover" period that follows alcohol intoxication and its subsequent clearance remain largely unknown. This is important because acute alcohol intoxication causes hormonal changes that could have longer-lasting effects on key metabolic tissues such as skeletal muscle. For instance, acute alcohol intoxication stimulates the hypothalamic-pituitary axis leading to a significant elevation in circulating glucocorticoids (corticosterone in rodents, cortisol in humans) (13). The acute release of glucocorticoids may alter fuel metabolism in skeletal muscle including decreased protein synthesis, induction of insulin resistance, and changes in circulating triglycerides, whereas longer lasting effects on skeletal muscle fuel metabolism may be induced by alterations to the metabolic gene expression signature (14–17). Such a change in whole body metabolism and the metabolic gene expression signature may contribute to the sustained decrease in task or muscular performance observed during the hangover period (18, 19).

Given the lack of information regarding metabolic shifts throughout the hangover period, the objective of this study was to define the metabolic aberrations during the hangover period following acute intoxication and assess how they coincide with sequential changes to transcription of metabolic genes in skeletal muscle. In addition, we tested whether the transient alcohol-induced rise in corticosterone is responsible for the early changes in the metabolic gene expression signature in skeletal muscle. Herein, we show that an acute alcohol binge shifts whole body metabolism in favor of fat oxidation for up to 48 h after the binge episode. These changes in metabolism coincided with a rapid change in the expression of genes and proteins involved in fat oxidation, carbohydrate utilization, and protein metabolism within the skeletal muscle and somewhat mimicked changes observed in response to food deprivation. Finally, we show that many of the early transcriptional changes related to fatty acid and glucose oxidation induced by alcohol are not mediated by corticosterone release following intoxication, though signals related to protein breakdown are altered by this hormone.

METHODS

Experimental Design

Experiment 1: Indirect calorimetry.

Animals. Fifteen-week-old female (n = 8) C57BL6/Hsd mice purchased from Envigo (Indianapolis, IN) were individually housed before the experiment in the vivarium at Florida State University in a temperature-controlled (25°C) room in a 12-h:12-h light/dark cycle with ad libitum access to water and chow (Lab Diet No. 5001). Due to their enhanced sensitivity to alcoholic disease, only female mice were used (20–22).

Mice were randomly assigned to Control (saline; n = 4) or Alcohol (EtOH; n = 4) while matching body weight between groups and were placed into cages of the Comprehensive Laboratory Animal Monitoring System (CLAMS; Columbus Instruments, Columbus, OH) to determine indirect calorimetry measurements. Oxygen consumption ($\dot{V}O_2$; mL/kg/h), carbon dioxide production ($\dot{V}CO_2$; mL/kg/h), respiratory exchange ratio (RER), heat (kcal/min), locomotor activity assessed via number of beam breaks, food intake, and water consumption were tracked for a total of 9 days, including 3 days of acclimation and 6 days of experimental data collection after treatment. Alcohol was administered via an intraperitoneal (IP) injection of either saline (CON) or alcohol (EtOH) at 5 g/kg (diluted to 31.5% solution) at the start of the dark cycle. Mice were briefly (1–2 min) removed from CLAMS cages for the injection and immediately placed back into the CLAMS cage, whereas data were continuously collected. Time points when the mouse was removed from the cage were not included in the final analysis. Food and water were provided ad libitum for the duration of the study. Data were collected in 30-s intervals representing an average value from that sampling period as calculated via the Oxymax software (CLAX; Columbus Instruments) from each cage (23). At the completion of the testing period, all data were exported and then analyzed using CLAX software. $\dot{V}O_2$ and $\dot{V}CO_2$ were used to calculate RER ($\dot{V}CO_2/\dot{V}O_2$), and carbohydrate oxidation and fat oxidation via the following equations (24):

Carbohydrate oxidation:

$$\left(4.585 \times \dot{V}CO_2\right) - \left(3.226 \times \dot{V}O_2\right)$$

Fat oxidation:

$$\left(1.695 \times \dot{V}O_2\right) - \left(1.701 \times \dot{V}CO_2\right)$$

Data were averaged into 3-h blocks and used for analysis.

Experiment 2: 0–24 h after acute alcohol intoxication.

Animals. The experimental design was previously described (13). Briefly, female (n = 39) C57BL6/Hsd mice (15 wk old) were purchased from Envigo (Indianapolis, IN) and housed at Florida State University in a temperature-controlled (25°C) room in a 12-h:12-h light/dark cycle with ad libitum access to food and chow (Lab Diet No. 5001). Mice were randomly assigned to one of three groups of equal body weight: Baseline (n = 3), Control (CON; n = 18), or Alcohol (EtOH; n = 18).

Experimental design. At the start of the dark cycle, gastrocnemius muscles (GAS) were collected from baseline mice, whereas control and alcohol mice received a 5 g/kg ip injection of saline or EtOH, respectively. The GAS muscle was then collected from three CON and three EtOH-treated mice every 4 h across a 24-h period. Gastrocnemius muscles and livers were immediately excised and frozen in liquid nitrogen until storage at −80°C for future analysis.

Blood was collected from an additional cohort of female C57BL6/Hsd mice (CON; n = 11; EtOH; n = 17) using the identical protocol design as aforementioned. Mice were euthanized under isoflurane at 30 min, 4 h, 8 h, and 12 h postinjection (CON n = 2–3; EtOH n = 3–5), and blood samples were collected. An aliquot was stored at room temperature for 30–60 min to allow for clotting and isolation of serum, whereas plasma aliquots were collected in EDTA-treated tubes and stored on ice until centrifugation and further storage at −80°C for future analysis. All procedures were approved by Animal Care and Use Committee at Florida State University and conformed to American Veterinary Medical Association (AVMA) guidelines.

Experiment 3: 24–48 h after alcohol intoxication.

As previously described (13), a follow-up experiment was conducted with female (n = 42) C57BL6/Hsd mice to extend our data collection period to include 24–48 h postintoxication. The methodology was identical to those described in *experiment 2*, except that tissue collection began 24 h after the injection of alcohol and continued every 4 h until 48 h postinjection. All procedures were approved by Animal Care and Use Committee at Florida State University and conformed to AVMA guidelines.

Experiment 4: Inhibition of corticosterone synthesis and the effects of alcohol intoxication.

Female C57BL/6Hsd mice (15 wk old), purchased from Envigo (Indianapolis, IN), were individually housed in the Florida State University vivarium for at least 2 wk before testing. Mice were then assigned to one of four groups matched for body weight: Control (CON; n = 5), Control + Metyrapone (Con-MET; n = 5), Alcohol (EtOH; n = 7), or Alcohol + Metyrapone (EtOH-MET; n = 7). Mice received a 100 mg/kg body wt ip injection of metyrapone (VWR, Cat. No. 101095-552) diluted in saline or saline alone (CON, EtOH). Ninety minutes after metyrapone treatment and at the start of the dark cycle, a 5 g/kg body wt ip injection of either saline (control) or alcohol (EtOH) was administered. All mice were euthanized 4 h later as aforementioned, and gastrocnemius muscles were collected and immediately frozen in liquid nitrogen and stored at −80°C. Blood was collected as aforementioned. All procedures were approved by Animal Care and Use Committee at Florida State University and conformed to AVMA guidelines.

Experiment 5: Determination of the influence of fasting on alcohol-induced changes in circulating substrates and skeletal muscle gene expression.

Female C57/BL6Hsd mice were purchased from Envigo (Indianapolis, IN) and were individually housed in the Florida State University vivarium for >1 wk before experimentation. Mice were then assigned to one of three groups matched for body weight: Control-fed (CON, n = 17), Control-Fasted (CON-FAST, n = 18), or Alcohol-fed (EtOH, n = 18). At the beginning of the dark cycle, all mice received an intraperitoneal injection of either 0.9% sterile saline (Control) or alcohol at a dose of 5 g/kg as described for *experiments 1–4*. Control-fed and EtOH-fed mice were allowed free access to chow and water ad libitum for the duration of the experiment. Control-fasted mice had their food removed at the beginning of the dark cycle at the time of injection and remained fasted for the remainder of the experiment (up to 20 h of fasting). Before anesthetization, body temperature was determined using a lubricated Thermocouple Thermometer (ST2-34-1401, Harvard Apparatus, Holliston, MA) and blood glucose was assessed using a Clarity blood glucose meter. Blood was also collected for insulin in heparin-coated capillary tubes before anesthetization. At 8, 12, 16, and 20 h after intoxication, animals were euthanized via isoflurane overdose and blood and gastrocnemius muscles were collected. Plasma was isolated from blood collected in EDTA-treated tubes and stored at −80°C. Glucose and insulin measurements at 4 h were taken from mice that were later euthanized at 8 h. Procedures for tissue collection during dark cycle times were identical to those aforementioned.

RNA extraction, cDNA synthesis, and RT-PCR. RNA extraction, cDNA synthesis, and RT-PCR protocols were previously described (13); briefly, the entire GAS was powdered in liquid nitrogen with mortar and pestle. From that, 20 mg of powder was homogenized in 600 μL of TRI reagent (Zymo Research, Irvine, CA). Similarly, a portion of the liver was homogenized in 600 μL of TRI reagent. RNA was isolated using the Direct-zol RNA MiniPrep kit (Zymo Research, Irvine, CA), and cDNA was synthesized using the High-capacity cDNA Reverse Transcription kit according to the manufacturer's instructions (Applied Biosystems, Foster City, CA). Relative mRNA expression was measured via RT-PCR using a QuantStudio3 and SYBR green master mix (Applied Biosystems, No. A25776). A melt curve analysis was performed for primer pairs to ensure a single product was amplified, and the appropriate product size was determined via gel electrophoresis. SYBR green primer sequences are referenced in Table 1. Measurement of Cullin1 (*Cul1*) (assay ID Mm00516318), pyruvate dehydrogenase kinase 4 (*Pdk4*) (assay ID Mm01166879), hexokinase 2 (*Hk2*) (assay ID Mm00443385), and Krupple-like factor 15 (*Klf15*) (assay ID Mm00517792) were quantified using TaqMan predesigned primer probes (Applied Biosystems) and TaqMan fast advanced master mix (Applied Biosystems, No. 4444557). Results were analyzed using the ΔΔCT method and referenced to either *Rplpo* or *Rpl26*, which did not change with treatment or time.

Western blotting and analysis. Western blotting was performed as previously described (13). Briefly, ∼40 mg of powdered GAS was homogenized in 10 volumes of buffer via glass-on-glass homogenization. Muscle extracts were centrifuged, and the supernatant was collected and quantified via Bradford method (Biorad, Cat. No. 5000006). Samples were diluted to the same concentration in 2× sample buffer. Blots were performed using either individual samples to determine changes at each time point or using samples from each time point pooled together with equal amounts of protein and volume to allow for the determination of overall circadian expression patterns, as previously described (25, 26). Proteins (25 μg) were fractioned on 4%–20% Biorad Criterion precast gels (Hercules, CA), transferred to PVDF membranes, and assessed for effective transfer and equal protein-loading via Ponceau-S staining. Membranes were blocked in 5% nonfat dried milk in Tris-buffered saline + 0.1% Tween20, and membranes were then incubated overnight at 4°C with antibodies against the following proteins from Cell Signaling Technology each diluted to 1:1,000 for use: AMPKα Thr172 (No. 2531), AMPKα (No. 2532), FOXO1 Ser256 (No. 9461), FOXO1 (No. 2880), CREB (No. 9197), and CREB p65 (No. 9198). As well as the following antibodies from the indicated company: GAPDH (Santa Cruz Biotech, No. sc-32233) diluted 1:40,000; PDK4 (Abcam, No. 214938) diluted 1:1,000; and MCT1 (NOVUS Biologicals, No. NPB1-59656) diluted 1:1,000. Appropriate secondary antibody was used at 1:10,000 (Bethyl Laboratories; No. A120-101 and No. A90-116), and the antigen-antibody complex was visualized by enhanced chemiluminescence using Clarity reagent (Bio-Rad) on a Bio-Rad ChemiDoc Touch imaging system. ImageJ software (National Institutes of Health, Bethesda, MD) was used to quantify images, including corresponding Ponceau-S stains.

Plasma β-hydroxybutyrate concentrations. A Precision Xtra monitoring system (Abbott, Columbus, OH) was used with blood β-ketone test strips to measure β-hydroxybutyrate levels from plasma samples taken from *experiments 1*, *2*, and *5*.

Table 1. *Primer sequences and amplicon size (base pairs) for SYBR green primers used for RT-PCR*

Gene Symbol	Forward (5′-3′)	Reverse (5′-3′)	Amplicon Size, bp
Bcat2	CAAGCCCTCCTGTACGTCAT	GCCACAGTGGGTCCATAGTT	158
Bhd1	ACCGACTGAGAACCATCCAG	ATGCTGGTGAACTCCACCTC	160
Cd36	AGTCCTGGCTGTGTTTGGAG	TGGGTTTTGCACATCAAAGA	169
Cebpß	CAAGCTGAGCGACGAGTACA	AGCTGCTCCACCTTCTTCTG	156
Dbt	CTGCTTCTCTGGGACTCCTG	GGACAATTAACCCCAGCTCA	129
Dgat2	CTGTCACCTGGCTCAACAGA	TATCAGCCAGCAGTCTGTGC	143
Fasn	TGGGTTCTAGCCAGCAGAGT	ACCACCAGAGACCGTTATGC	158
Foxo1	TTTCTAAGTGGCCTGCGAGT	GGTGGATACACCAGGGAATG	175
Foxo3a	AGCCGTGTACTGTGGAGCTT	TCTTGGCGGTATATGGGAAG	180
Gck	CGTGAAGACGAAACACCAGA	AGGGAAGGAAGGGGTGAAGC	160
Hadh	ACCAAACGGAAGACATCCTG	AGCTCAGGGTCTTCTCCACA	126
Idh1	AGGTTCTGTGGTGGAGATGC	TCTGCAGCATCTTTGGTGAC	165
Mafbx	GTCGCAGCCAAGAAGAGAAAG	ACTCAGGGATGTGAGCTGTGA	240
Murf1	AAGCAGGAGTGCTCCAGTCG	AACAGCATGGAGATGCAGTTAC	217
Nadsyn	GAGCCTTTGTCCAGTTTTGC	GCCGAAGATGGAGAGTTCTG	164
Nampt	AGTGGCCACAAATTCCAGAG	CAATTCCCGCCACAGTATCT	194
Oxct1	TGCCTTCTACACCAGCACAG	GATGGCTTCCTCCAAAATGA	151
Pck1	GCAGAACACAAGGGCAAGAT	CTTCCGGAACCAGTTGACAT	156
Pkfm	GGAGTGCGTGCAGGTGACCAAA	ATCACGGCCACTGTGTGCAACC	171
Pparα	ATGCCAGTACTGCCGTTTTC	CCGAATCTTTCAGGTCGTGT	140
Pparδ/β	TGGAGCTCGATGACAGTGAC	GTACTGGCTCTGAGGGTGGT	161
Rpl26	TGTTCGCGGACACTACAAAG	CGGTCCTTGTCCAGCTTTAG	174
Rplpo	CAACCCAGCTCTGGAGAAAC	GTTCTGAGCTGGCACAGTGA	169
Sirt1	AGTTCCAGCCGTCTCTGTGT	CTCCACGAACAGCTTCACAA	198

NAD+/NADH assay. The concentration of NAD+ and NADH in gastrocnemius at 16 and 20 h after intoxication was determined using a commercially available kit (Abcam, Cambridge, UK, ab65348) as per the manufacturers' instructions. Briefly, powdered gastrocnemius (~10–15 mg) was homogenized in 400 µL of NADH/NAD extraction buffer on ice using the glass-on-glass technique. Homogenates were then centrifuged at 15,000 *g* for 5 min at 4°C, and ~300 µL of supernatant was collected from each sample. The supernatant was passed through 10 kD spin columns (Abcam Cat. No. ab93349) by centrifugation at 15,000 *g* for 90 min at 4°C. The resultant extract was the total NAD+ sample, and from this extract, 50 µL was placed on the heat block at 60°C for 30 min to produce the NAD+ decomposition (NAD decomp) product. The NAD+ total samples were diluted at 1:30 and the NAD decomp samples were diluted at 1:10 in NADH/NAD+ extraction buffer before initiating the final reaction and reading plate at 450 nm every 10 min until all samples fell within the standard curve. Data are presented as means ± standard deviation.

Plasma insulin. Plasma insulin concentrations from *experiment 5* were measured using the Ultra Sensitive Mouse Insulin ELISA kit (Crystal Chem, Elk Grove Village, IL) as per the manufacturers' instructions. Data are presented as means (Measure A_{450} − Measure A_{630}) ± standard deviation.

Free fatty acid assay. Plasma free fatty acids from *experiment 5* were determined via the Free Fatty Acid Assay kit (Abcam, Ab65341) as per the manufacturers' instructions and using undiluted plasma samples. Free fatty acid concentrations were calculated via the equation: (amount of fatty acid in sample calculated from standard curve/sample volume added in wells) × sample dilution factor. Data are presented as means ± standard deviation.

Statistical analysis. Data are expressed as means ± standard deviations (SD), except for diurnal protein patterns, which are expressed as single data points due to pooling of samples. A two-way ANOVA was used to analyze whole body metabolism, mRNA expression, protein expression, and plasma metabolites using EtOH and time as the two factors. A two-way ANOVA (EtOH, Met) was used to analyze mRNA and protein expression in the metyrapone study using alcohol and metyrapone as the two factors. In the event of a significant interaction, differences between multiple comparisons were identified using Sidak's post hoc correction, otherwise, only main effects are reported. NAD+, NADH, and NAD+/NADH ratio, as well as AMPK protein content within each time point, were analyzed using Student's *t* test. For *experiment 5*, a one-way ANOVA with Tukey's post hoc test when appropriate was performed between CON-FED, CON-FAST, and EtOH-FED at each time point for the following variables: blood glucose, body temperature, plasma insulin, plasma free fatty acids, and gastrocnemius muscle gene expression. Significance was set to $P < 0.05$ for all analyses. All analyses were performed using GraphPad Prism Software (San Diego, CA).

RESULTS

Alcohol Alters Whole Body Fuel Metabolism for Several Days following a Single Binge

RER ($P < 0.0001$), $\dot{V}O_2$ ($P < 0.0001$), heat ($P < 0.0001$), and locomotor activity ($P < 0.0001$) were reduced within 4 h of EtOH treatment (Fig. 1, *A–D*). RER remained lower in EtOH-treated mice up to ~72 h post EtOH binge even though alcohol is completely cleared from circulation within ~12 h (13). Coinciding with the reductions in RER, acute alcohol intoxication enhanced fat oxidation (P = 0.01) and suppressed carbohydrate oxidation ($P < 0.0001$) for at least 3 days following intoxication (Fig. 1, *E* and *F*). Despite no main effect of alcohol intoxication being statistically detected, a reduction in food and water intake was clearly evident immediately

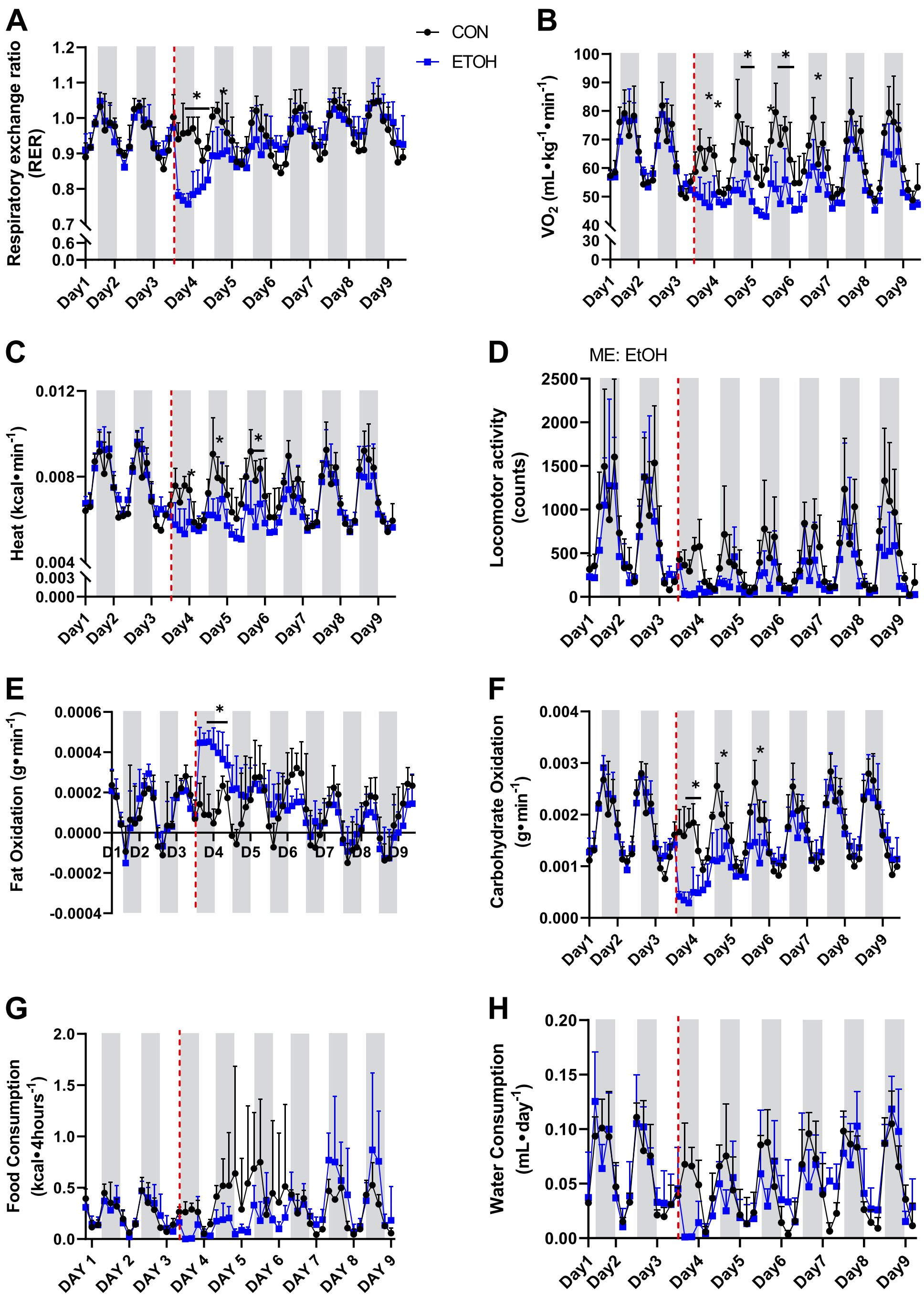

Figure 1. The effects of acute alcohol intoxication on measures of whole body metabolism including respiratory exchange ratio (RER) (*A*), $\dot{V}O_2$ (*B*), heat (*C*), locomotor activity (*D*), fat oxidation (*E*), carbohydrate oxidation (*F*), food consumption (*G*), and water consumption (*H*) measured via the Comprehensive Laboratory Animal Monitoring System (CLAMS). Black circles represent control (CON; n = 4), whereas blue squares represent alcohol (EtOH; n = 4). The red dashed line represents the time of the EtOH (5 g/kg) injection, with the time points to the left representing acclimation days and the time points to the right representing postbinge data collection. The data are shown as average of every 3 h ± standard deviation (SD) over an ~9-day collection period. The gray shading depicts the dark cycle [Zeitgeber (ZT) 0–12)], and open area the light cycle (ZT 12–24). Two-way ANOVA was preformed (Time, EtOH) where $P \leq 0.05$, with Sidak post hoc testing when a significant interaction was present. The main effect of alcohol is displayed as ME:EtOH and when there is a significant interaction between time and EtOH, differences between Control and EtOH are indicated by (*).

following the intoxication period (Fig. 1, *G* and *H*). Food intake did not return to normal levels until ~48 h after intoxication (*day 5*), whereas rhythmic water intake was not normalized until ~72 h after intoxication (*day 7*). The lack of statistical significance was likely due to the high number of comparisons performed to analyze the data over the 9-day collection period as well as the variability between animals following intoxication.

Binge Alcohol Increases NAD + /NADH in Skeletal Muscle and Levels of Circulating Ketones

To investigate the skeletal muscle metabolic response to binge alcohol further, targets sensitive to changes in macronutrient energy availability were probed. Despite little change in AMPKα T172 phosphorylation following alcohol intoxication (Supplemental Fig. S1), the NAD+ to NADH ratio 16–20 h after intoxication was increased as was the mRNA expression of *Nampt* (P = 0.002, 0–24 h; $P < 0.0001$, 24–48 h) and NAD synthetase 1 (*Nadsyn1*) starting 12 h after intoxication (Fig. 2, *A–C*). The increase in NAD+, which serves as a cosubstrate for sirtuin-mediated deacetylation, was also in line with an increase in *Sirt1* mRNA expression at 12–20 h (Fig. 2*D*). In contrast, mRNA expression of PPAR-γ coactivator-1 α, a SIRT1 substrate, was unchanged following alcohol intoxication (data not shown); however, acetylation status of the protein was not assessed.

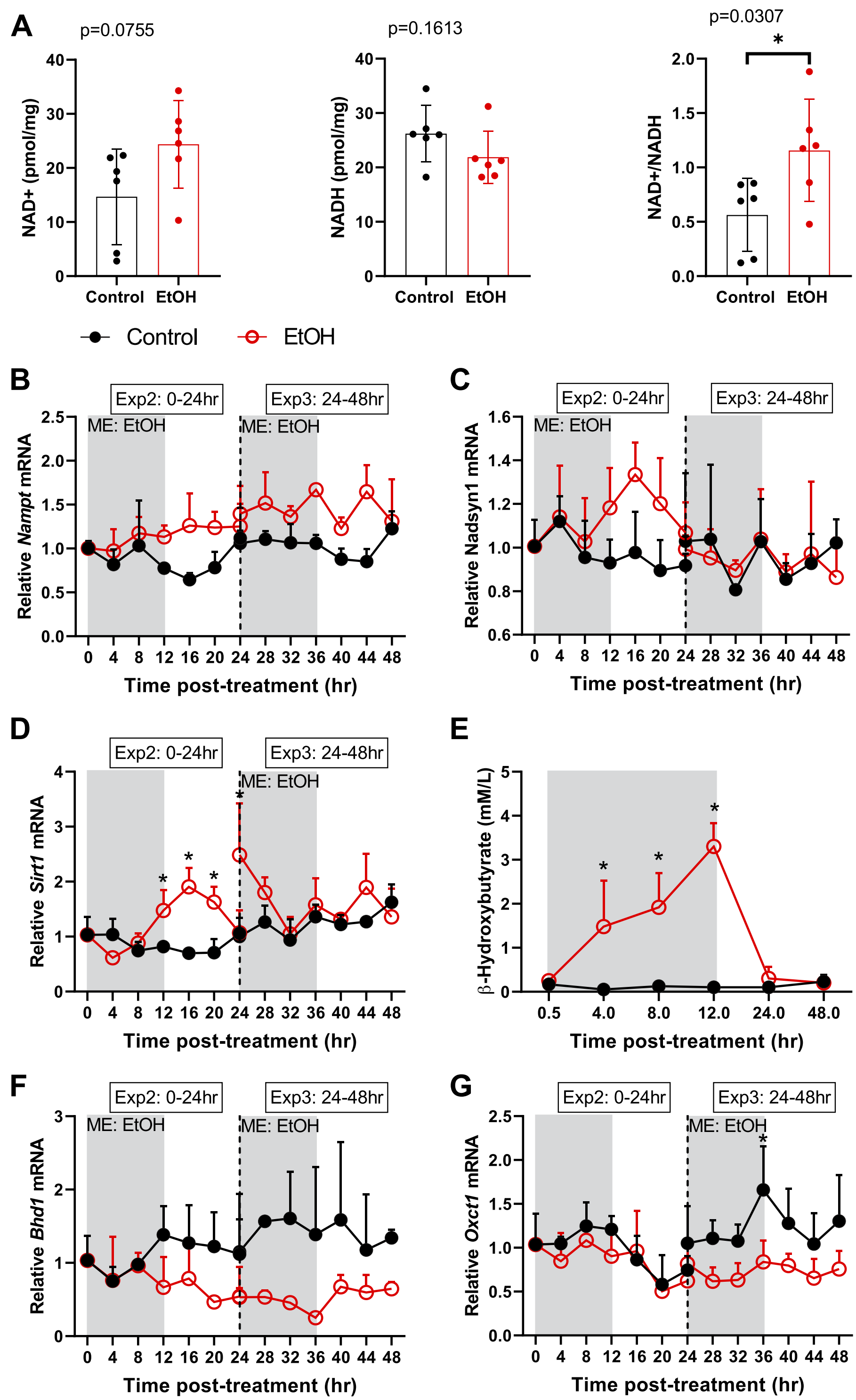

Figure 2. The effects of acute alcohol intoxication on nutrient sensing pathways including NAD+, NADH, NAD+/NADH ratio (*A*), *Nampt* (*B*), *Nadsyn1* (*C*), and *Sirt1* (*D*), and its effects on plasma β-hydroxybutyrate (*E*), and ketolytic genes, *Bdh1* (*F*), and *Oxct1* (*G*) in the gastrocnemius. Data are from *experiment 2* (0–24 h) and *experiment 3* (24–48 h). The vertical dotted line represents the division of the two experiments, and gray shading shows the dark cycle (0–12 h, 24–36 h), whereas white boxes indicate the light cycle (12–24 h, 36–48 h). The 0-h time point is the time of injection and baseline tissue collection (n = 3). The black spheres represent control (n = 3), and the open red spheres represent EtOH (n = 3). Data are presented as means ± SD for each time point. Main effects and interactions were determined by two-way ANOVA (Time, EtOH) where $P \leq 0.05$, and the main effect of alcohol is displayed on the graph as ME:EtOH. When there is a significant interaction between Time and EtOH, differences between Control and EtOH are indicated by (*).

When glucose levels are inadequate, ketones can be produced by the liver to be used as an alternative fuel source by extrahepatic metabolic tissues like the skeletal muscle. Presently, plasma β-hydroxybutyrate levels ($P < 0.0001$) were increased at 4 h postbinge and remained elevated at 8 and 12 h as well (Fig. 2*E*). Two ketolytic genes, hydroxybutyrate dehydrogenase 1 (*Bdh1*) and oxoacid CoA-transferase 1 (Oxct1) were decreased from either 12–48 h (Bdh1) or 28–48 h postintoxication (Fig. 2, *F* and *G*); however, monocarboxylate transporter 1 (MCT1) protein was unchanged with acute alcohol intoxication (Supplemental Fig. S2).

Binge Alcohol Results in a Rapid Change to the Metabolic Gene Expression Signature in Skeletal Muscle That is Consistent with Enhanced Fat Oxidation

The mRNA content of the fatty acid transporter, Cluster of Differentiation 36 (*Cd36*) was markedly increased from 12–44 h (P = 0.001, 0–24 h; $P < 0.0001$, 24–48 h) following alcohol intoxication (Fig. 3*A*), whereas lipoprotein lipase (*Lpl*), which mediates the breakdown of fatty acids to fatty acyl-CoA, was not altered by alcohol (data not shown). Hydroxyacyl-coenzyme A dehydrogenase (*Hadh*), which catalyzes the third step of β-oxidation in the mitochondria, was also not significantly changed by alcohol intoxication despite a nonsignificant increase 8–16 h after intoxication (Fig. 3*B*). Conversely, fatty acid synthase (*Fasn*), which converts acetyl CoA and malonyl CoA to palmitate, was lower in alcohol-treated muscle compared with control for the entire 48-h measurement period (P = 0.001, 0–24 h; P = 0.02, 24–48 h) (Fig. 3*C*).

Peroxisome proliferator-activated receptor delta/beta (*Ppar*δ/β) mRNA, which can enhance *Cd36* as well as fatty acid oxidation, was rapidly induced and remained elevated throughout most of the sampling period ($P < 0.0001$, 0–24 h; $P < 0.0001$, 24–48 h) (Fig. 3*D*). Similarly, *Ppar*α mRNA was increased at 4 and 8 h after intoxication before being decreased at 32 h (P = 0.003, 0–24 h; P = 0.02, 24–48 h) (Fig. 3*E*). *Ppar*δ/β can enhance the expression of Forkhead box O1 (*FoxO1*), a transcription factor central to macronutrient metabolism, especially under conditions of metabolic dysfunction (27, 28). *FoxO1* mRNA expression was increased in the first 16 h after alcohol intoxication ($P < 0.001$, 0–24 h; P = 0.19, 24–48 h) (Fig. 3*F*), whereas FOXO1 Ser256 phosphorylation was suppressed over the entire 48-h period indicative of enhancement of FOXO1 activity which can increase lipid oxidation via LPL and CD36 (Fig. 3, *G* and *H*).

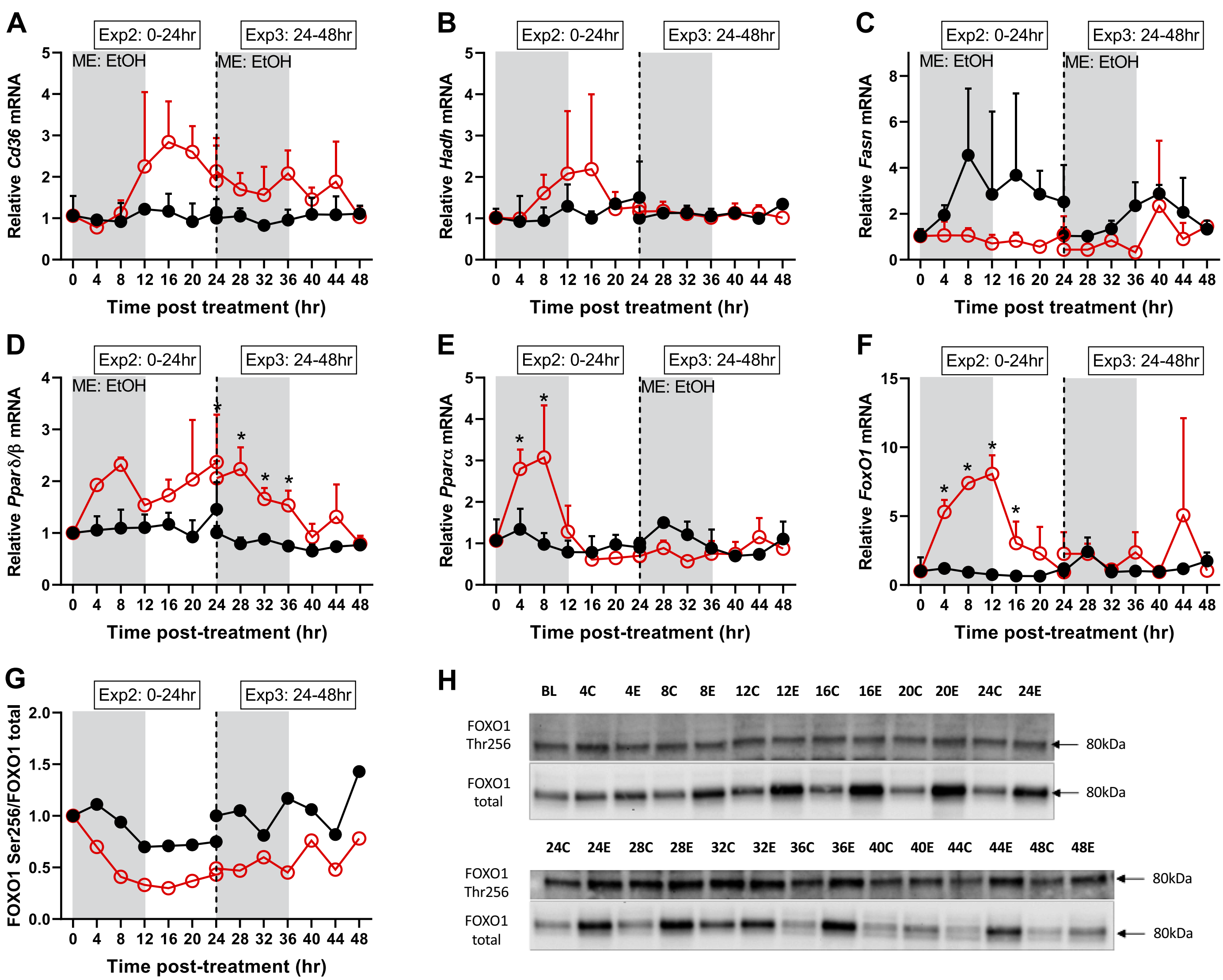

Figure 3. The effects of acute alcohol intoxication on genes involved in lipid metabolism including *Cd36* (*A*), *Hadh* (*B*), *Fasn* (*C*), *Ppar*δ/β (*D*), *Ppar*α (*E*), *FoxO1* (*F*), FOXO1 Ser256/FOXO1 total (*G* and *H*) from *experiment 2* (0–24 h) and *experiment 3* (24–48 h) for gastrocnemius. The vertical dotted line represents the division of the two experiments, and gray shading shows the dark cycle (0–12 h, 24–36 h), whereas white boxes indicate the light cycle (12–24 h, 36–48 h). The 0-h time point is the time of injection and baseline tissue collection (n = 3). The black spheres represent control (n = 3), and the open red spheres represent EtOH (n = 3). Data are presented as means ± SD for each time point. Main effects and interactions were determined by two-way ANOVA (Time, EtOH) where $P \leq 0.05$, and the main effect of alcohol is displayed on the graph as ME:EtOH. When there is a significant interaction between Time and EtOH, differences between Control and EtOH are indicated by (*). Western blots are labeled above with the hour and then treatment (C for control and E for alcohol) corresponding to the band below it. BL stands for baseline.

Binge Alcohol Results in a Rapid Change to the Metabolic Gene Expression Signature in Skeletal Muscle That is Consistent with Decreased Carbohydrate Oxidation

Expression of hexokinase (*Hk2*), a rate-limiting enzyme of glycolysis that phosphorylates glucose to glucose-6-phosphate, was not changed by alcohol intoxication (Fig. 4*A*). Similarly, expression of phosphofructokinase, muscle (*Pfkm*), the rate-limiting enzyme responsible for the conversion of fructose-6 phosphate to fructose-1,6-bisphosphate during glycolysis, was unchanged in the first 24 h after alcohol, before being decreased throughout the second dark cycle (28–36 h) (P = 0.40, 0–24 h; P = 0.001, 24–48 h) (Fig. 4*B*). Conversely, pyruvate dehydrogenase 4 (*Pdk4*) mRNA expression, whose mRNA expression is regulated in part by PPARα as well as PPARδ/β and CD36 (29, 30), was markedly increased from 8 to 20 h ($P < 0.0001$, 0–24 h; P = 0.06, 24–48 h). This change in *Pdk4* mRNA coincided with a rapid and sustained elevation in PDK4 protein, indicating inhibition of pyruvate dehydrogenase activity and subsequent glucose oxidation, as PDK4 suppresses the activity of the pyruvate dehydrogenase complex and limits the conversion of pyruvate to acetyl CoA (Fig. 4, *C, D,* and *G*). Similarly, the expression of phosphoenolpyruvate carboxykinase 1 (*Pck1* or *PEPCK*), which regulates the conversion of oxaloacetate (OAA) to phosphoenolpyruvate (PEP), was enhanced by alcohol intoxication between 4 and 12 h, with no changes at 24–48 h (P = 0.001, 0–24 h; P = 0.39, 24–48 h) (Fig. 4*E*). The increase in *Pck1* mRNA likely occurred in part by increased transcriptional activity of one of its regulators, cAMP-response element-binding protein (CREB), whose phosphorylation on the Ser133 activation site was elevated at similar time points (Fig. 4, *F* and *G*).

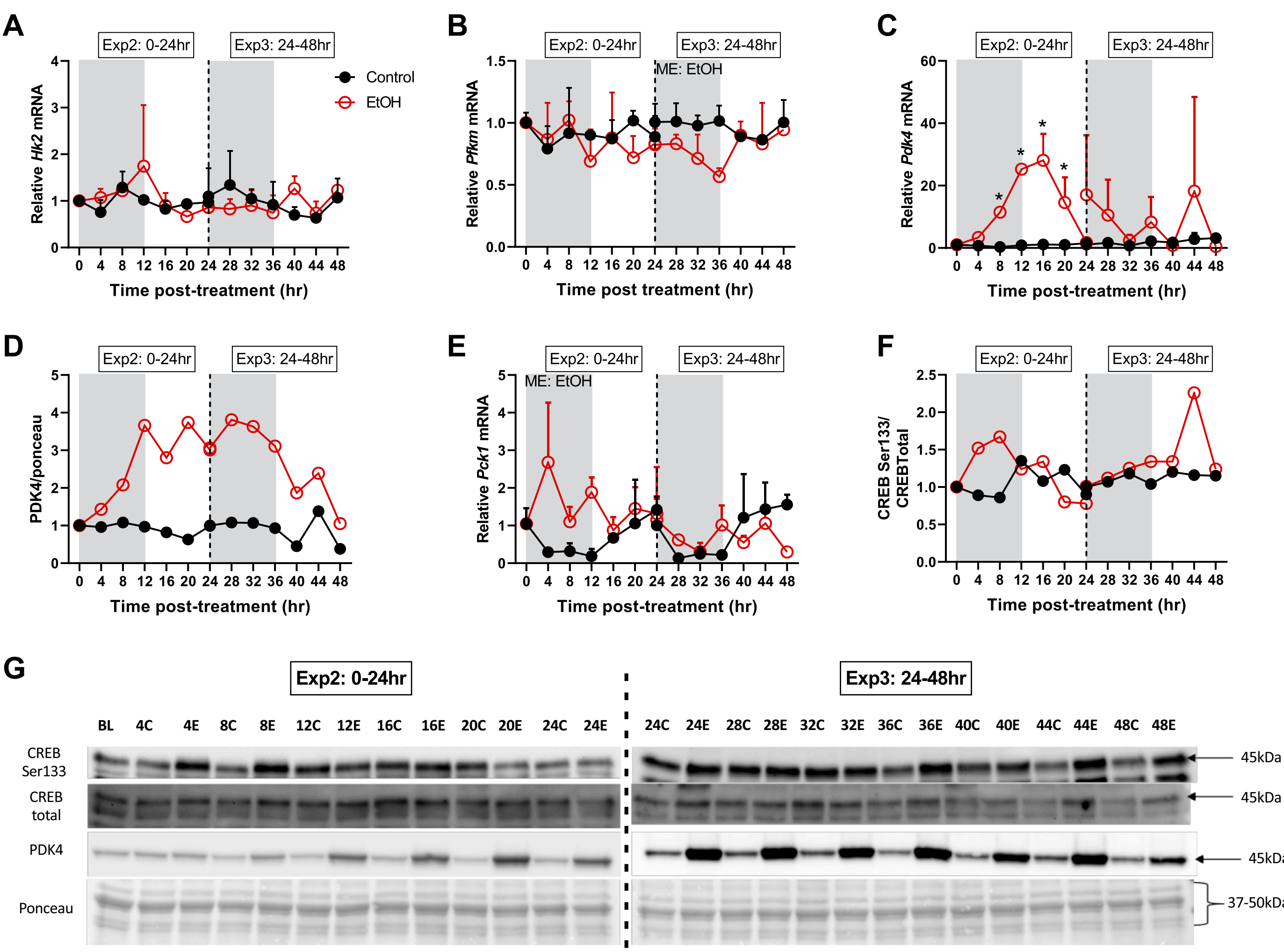

Figure 4. The effects of acute alcohol intoxication on glycolytic genes and proteins including *Hk2* (*A*), *Pfkm* (*B*), *Pdk4* (*C*), PDK4/Ponceau (*D* and *G*), *Pck1* (*E*), and CREB Ser133/CREB total (*F* and *G*), from *experiment 2* (0–24 h) and *experiment 3* (24–48 h) for gastrocnemius. The vertical dotted line represents the division of the two experiments, and gray shading shows the dark cycle (0–12 h, 24–36 h), whereas white boxes indicate the light cycle (12–24 h, 36–48 h). The 0-h time point is the time of injection and baseline tissue collection (n = 3). The black spheres represent control (n = 3), and the open red spheres represent EtOH (n = 3). Data are presented as means ± SD for each time point. Main effects and interactions were determined by two-way ANOVA (Time, EtOH) where $P \leq 0.05$, and the main effect of alcohol is displayed on the graph as ME:EtOH. When there is a significant interaction between Time and EtOH, differences between Control and EtOH are indicated by (*). Western blots are labeled above with the hour and then treatment (C for control and E for alcohol) corresponding to the band below it. BL stands for baseline.

Alcohol Intoxication Promotes Markers of Skeletal Muscle Protein Catabolism Favoring Amino Acid Release

Under catabolic conditions, protein breakdown is enhanced to provide amino acids for gluconeogenesis and a similar effect is stimulated by acute alcohol intoxication. Acute alcohol intoxication increased Muscle RING finger protein 1 (*Murf1*) mRNA ($P < 0.001$, 0–24 h; $P = 0.01$, 24–48 h), including a ∼35-fold increase compared with control at 12 h and 16 h postbinge (Fig. 5*A*). Muscle atrophy F-box (MAFbx) and its binding partner, Cullin1 (*Cul1*), exhibited increased mRNA expression following acute alcohol intoxication, with *Mafbx* increasing from 12 to 36 h ($P < 0.0001$, 0–24 h; $P = 0.0001$, 24–48 h) and Cul1 increasing from 20 to 44 h ($P = 0.003$, 0–24 h; $P < 0.0001$, 24–48 h) (Fig. 5, *B* and *C*). Furthermore, CCAAT enhancer-binding protein β (*Cebpβ*), known to enhance *Mafbx* mRNA expression, was increased with alcohol intoxication ($P = 0.22$, 0–24 h; $P = 0.004$, 24–48 h) (Fig. 5*D*). Finally, overall protein ubiquitination was increased 16–48 h after acute alcohol intoxication (Supplemental Fig. S3).

In further support of enhanced protein breakdown was the observed increase in mRNA content of *Klf15* ($P = 0.005$, 0–24 h; $P = 0.29$, 24–48 h) and its target, branched-chain amino acid (BCAA) transaminase 2 (*Bcat2*), which catalyzes the breakdown of BCAAs to branch chain keto acids (BCKAs) ($P = 0.001$, 0–24 h; $P = 0.0003$, 24–48 h) (Fig. 5, *E* and *F*). The conversion of BCAAs to BCKAs requires the donation of a ketoacid group, usually from α-ketoglutarate produced from isocitrate. This reaction is catalyzed by isocitrate dehydrogenase 1 (*Idh1*), which was increased by alcohol in the first 24 h before decreasing at 24–48 h ($P = 0.0003$, 0–24 h; $P < 0.0001$, 24–48 h) (Fig. 5*G*). The E2 ligase dihydrolipoamide branched chain transacylase E2 (*Dbt*) is a key component of the BCKA dehydrogenase (BCKDH) enzyme complex, a group of ubiquitin ligases involved in the breakdown of BCKAs to NADH, acyl-CoA, and CO_2. Accordingly, acute alcohol increased *Dbt* mRNA from 16 to 48 h following intoxication ($P = 0.0002$, 0–24 h; $P < 0.0001$, 24–48 h) (Fig. 5*H*).

Alcohol-Induced Elevation in Serum Corticosterone Enhances Catabolic Signals but Not the Expression of Genes Associated with Fatty Acid Oxidation

The rapid elevation in serum corticosterone levels that occurs in response to acute alcohol intoxication coincided with the rapid change in expression of genes that promote fatty acid oxidation, including genes that are well-defined targets of the glucocorticoid receptor (31). Although metyrapone effectively prevented the alcohol-mediated increase in serum corticosterone (13), *Klf15* mRNA was still induced by alcohol intoxication albeit to a lesser extent (Fig. 6*A*, Supplementary Fig. S4). The expression of other putative glucocorticoid target genes, *Cebpβ*, *Pparα,* and *FoxO1*, was increased by alcohol independent of the release of corticosterone (Fig. 6, *B–D*, Supplemental Fig. S4). Similarly, phosphorylation of FOXO1 Ser256 was not recovered with metyrapone treatment; however, metyrapone administered to control mice also decreased phosphorylation on this site precluding definitive conclusions from being drawn (Fig. 6*E*, Supplemental Figs. S4 and S5). In contrast, the alcohol-mediated increase in *FoxO3a* and *Murf1* mRNA expression was prevented by metyrapone (Fig. 6, *F* and *G*).

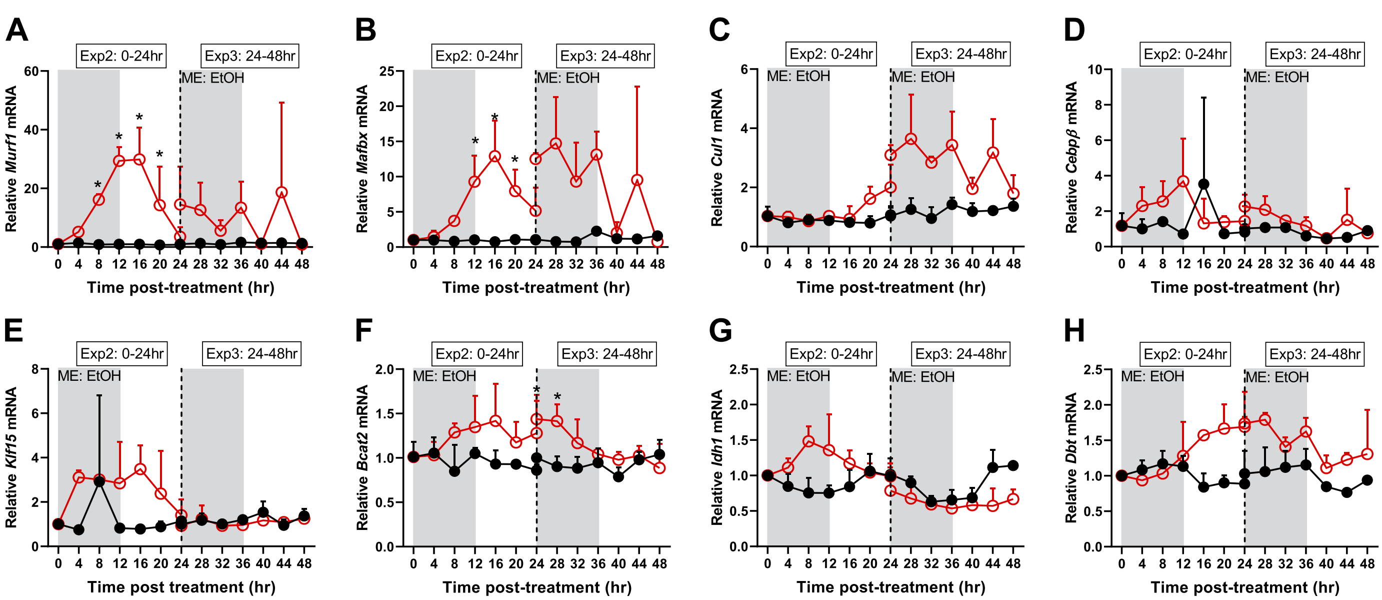

Figure 5. The effects of acute alcohol intoxication on catabolic components *Murf1* (*A*), *Mafbx* (*B*), *Cul1* (*C*), *Cebpβ* (*D*), *Klf15* (*E*), *Bcat2* (*F*), *Idh1* (*G*), and *Dbt* (*H*) from *experiment 2* (0–24 h) and *experiment 3* (24–48 h) for gastrocnemius. The vertical dotted line represents the division of the two experiments, and gray shading shows the dark cycle (0–12 h, 24–36 h), whereas white boxes indicate the light cycle (12–24 h, 36–48 h). The 0-h time point is the time of injection and baseline tissue collection ($n = 3$). The black spheres represent control ($n = 3$), and the open red spheres represent EtOH ($n = 3$). Data are presented as means ± SD for each time point. Main effects and interactions were determined by two-way ANOVA (Time, EtOH) where $P \leq 0.05$, and the main effect of alcohol is displayed on the graph as ME:EtOH. When there is a significant interaction between Time and EtOH, differences between Control and EtOH are indicated by (*).

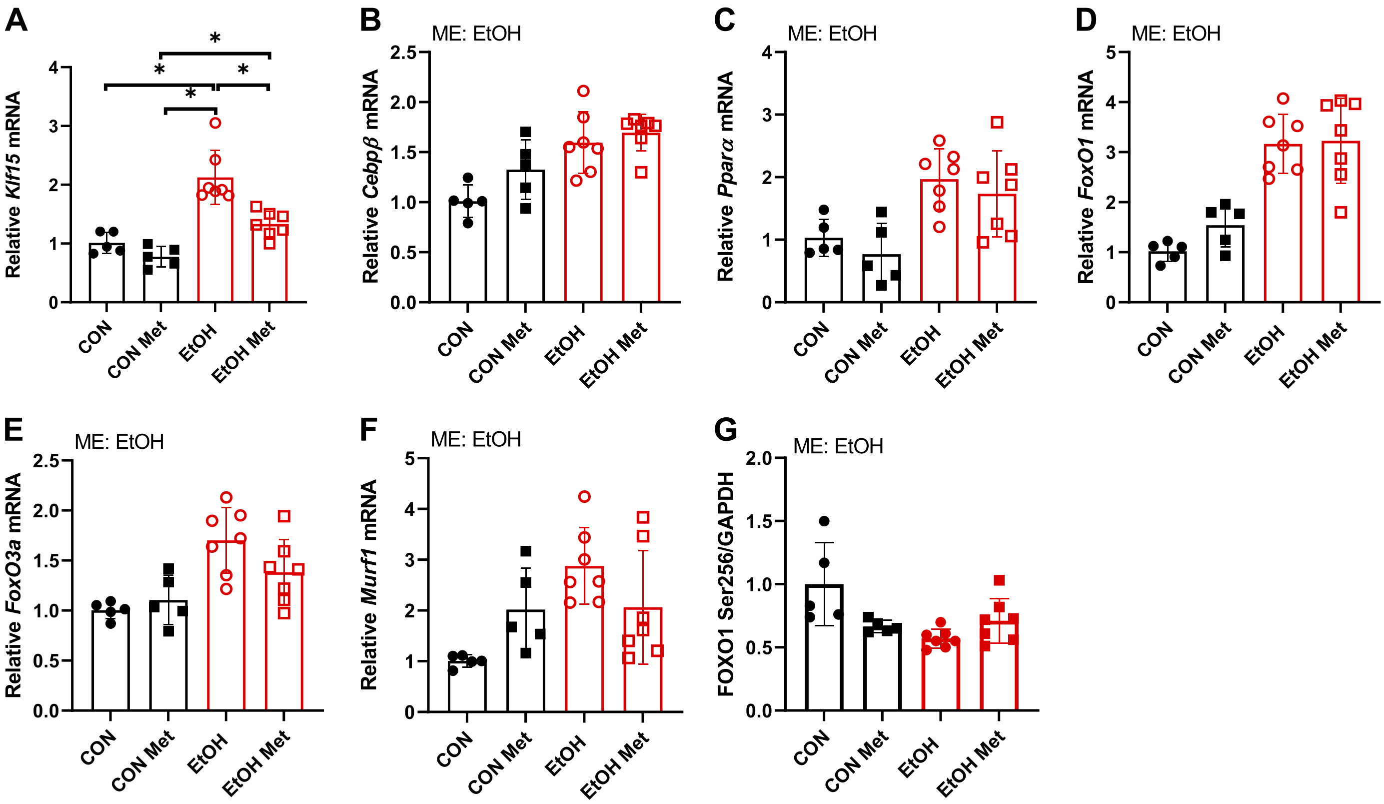

Figure 6. The effects of metyrapone treatment with acute alcohol intoxication on gastrocnemius *Klf15* (*A*), *Cebpβ* (*B*), *Pparα* (*C*), *Foxo1* (*D*), *Foxo3a* (*E*), *Murf1* (*F*), and FOXO1 Ser256/GAPDH (*G*) from *experiment 4*. Data from EtOH and EtOH-Met are normalized to the control group not receiving metyrapone. Black circles represent control (n = 5), black squares are control + metyrapone (n = 5), red open circles are ethanol (n = 7), and red open squares indicate ethanol + metyrapone (n = 7). Data are presented as means ± SD for each time point. Main effects and interactions were determined by two-way ANOVA (EtOH, Metyrapone) where $P \leq 0.05$, and the main effect of alcohol is displayed on the graph as ME:EtOH. When there is a significant interaction between Time and EtOH, differences between Control and EtOH are indicated by (*).

Fasting Induces a Similar, yet Distinct Metabolic Phenotype to Acute Alcohol Intoxication

As the rapid shift in the preferential use of lipids in response to alcohol intoxication observed in *experiment 1* is similar to the skeletal muscle's metabolic response to fasting despite the presence of significant energy from alcohol (7 kcal/g), additional experiments were performed to determine the possible role of reduced food intake on the response to alcohol intoxication. A cohort of time-matched fasted animals was included for comparison to alcohol-treated mice. Core body temperature was decreased by alcohol at 4 h and 8 h compared with control-fed and control-fasted mice but had normalized by 12 h after intoxication corresponding with the clearance of alcohol and a return of BAC to zero (data not shown) (Fig. 7*A*). Blood glucose was decreased by fasting (P = 0.03) and alcohol (P = 0.003) at 4 h and further reduced by alcohol at 8 h after binge ($P \leq 0.0001$) (Fig. 7*B*). At 12 h, blood glucose in alcohol-treated mice was not different than control-fed or control-fasted mice (Fig. 7*B*). At 16 and 20 h after intoxication, control-fasted had significantly lower blood glucose than control-fed and alcohol-treated mice (Fig. 7*B*). Plasma insulin concentrations were reduced at 4 h, 12 h, and 20 h posttreatment in control-fasted (P = 0.001, 0.003, 0.02) and alcohol-treated (P = 0.01, 0.01, 0.04) mice compared with control-fed animals (Fig. 7*C*). Plasma FFA concentrations were increased at 8 h postbinge with alcohol (P = 0.01) and at 16 h into fasting (P = 0.01) compared with control-fed mice (Fig. 7*D*). Finally, plasma β-hydroxybutyrate was increased in control-fasted mice at 4 h ($P < 0.0001$), 8 h (P = 0.0002), 16 h (P = 0.02), and 20 h (P = 0.01), whereas alcohol only increased ketones at 4 h ($P < 0.0001$) and 8 h ($P < 0.0001$) compared with fed controls (Fig. 7*E*). By 20 h, the fasting-induced increase in β-hydroxybutyrate was significantly greater than levels in alcohol-treated mice (P = 0.04) (Fig. 7*E*).

A select set of fasting-sensitive genes was also measured in the gastrocnemius to determine whether alcohol and fasting induced similar molecular changes. *Sirt1* mRNA was increased by fasting (P = 0.03, 0.005, 0.03) at 12, 16, and 20 h, and from alcohol at 12 and 16 h postbinge (P = 0.002, 0.04) compared with control-fed mice (Fig. 8*A*). Furthermore, *Foxo1* mRNA expression was enhanced with fasting (P = 0.01, 0.02) and alcohol (P = 0.002, 0.01) at 8 and 12 h compared with control-fed mice, whereas fasting alone increased *Foxo1* mRNA expression at 20 h (P = 0.01) compared with control-fed mice (Fig. 8*B*). *Pdk4* mRNA expression was increased with alcohol (P = 0.0002) compared with control-fed mice at 8 h postbinge. Fasting further increased *Pdk4* expression at 8 h compared with control-fed ($P < 0.0001$) and alcohol-treated (P = 0.003) mice. From 12 to 16-h posttreatment, *Pdk4* mRNA was increased with both fasting (P = 0.0001, 0.001) and alcohol ($P < 0.0001$, 0.02) compared with control

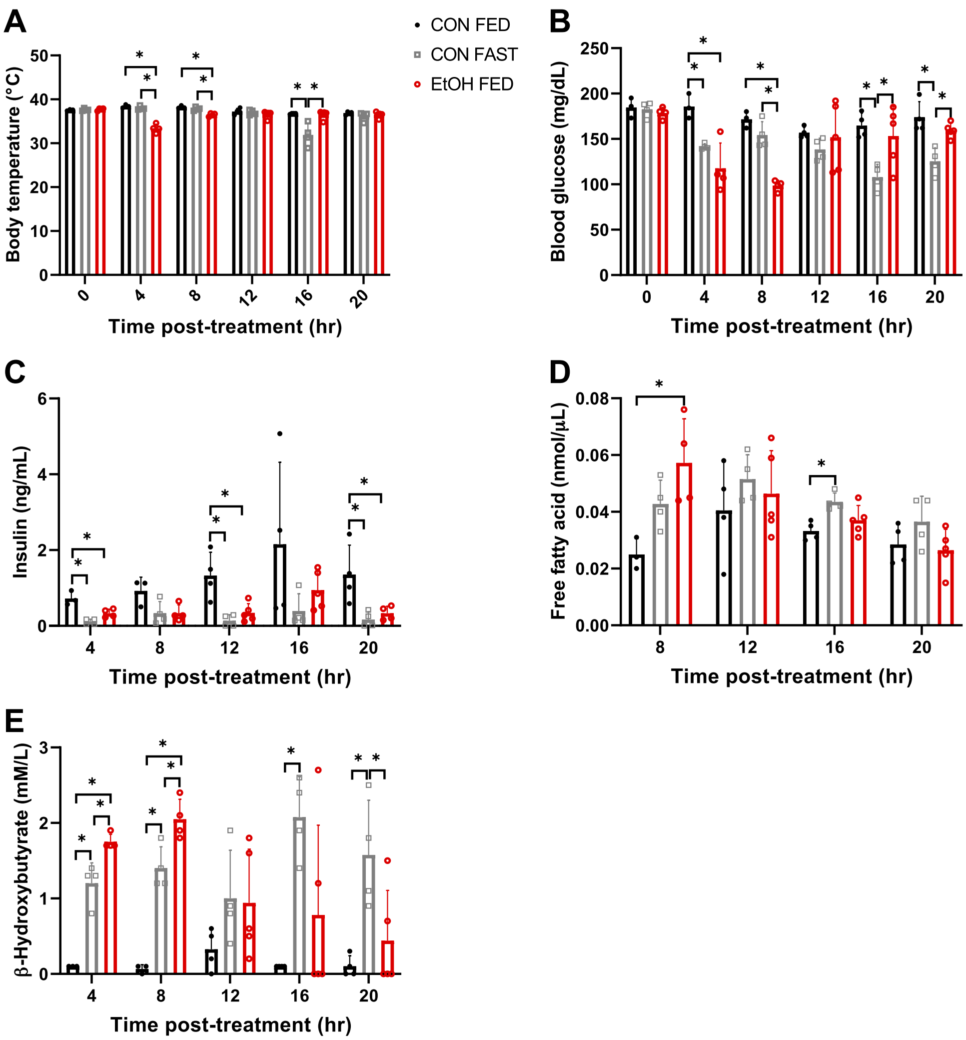

Figure 7. Determination of the potential influence of fasting on alcohol induced changes in body temperature (*A*) and circulating substrates, including blood glucose (*B*), plasma insulin (*C*), plasma free fatty acids (*D*), and plasma β-hydroxybutyrate (*E*). The black spheres represent control-fed (CON FED; n = 3–4), the gray open squares are control-fasted (CON FAST; n = 4), and the red open spheres are alcohol-fed (EtOH FED; n = 4–5). Data are presented as means ± SD for each time point. One-way ANOVA was performed to determine differences between groups at each time point where $P \leq 0.05$. *Significant difference between groups connected by horizontal lines.

fed; however, at 20 h, *Pdk4* was only increased in control-fasted muscle (P = 0.04) (Fig. 8*C*). *Murf1* mRNA expression was increased by fasting or alcohol at 8, 12, 16, and 20 h, whereas at 16 h, expression was lower in alcohol-treated mice compared with control-fasted mice (P = 0.002) (Fig. 8*D*). *Mafbx* was also increased with fasting and alcohol treatment at 8 h (P = 0.001, 0.03), 12 h ($P < 0.0001$, < 0.0001), 16 h ($P < 0.0001$, 0.01), and 20 h (P = 0.01, 0.01). However, fasting levels of *Mafbx* were significantly increased compared with alcohol mice at 8 h (P = 0.03) and 16 h (P = 0.01) post-treatment (Fig. 8*E*). Fasting increased *Cebp1β* at 8 h (P = 0.001), 12 h ($P < 0.0001$), 16 h (P = 0.001), and 20 h ($P < 0.0001$) compared with control-fed mice, whereas alcohol-treatment resulted in increased *Cebp1β* at 8 h (P = 0.0004), 12 h ($P < 0.0001$), 16 h (P = 0.01), and 20 h (P = 0.01). At 20 h into the fasting treatment, *Cebp1β* mRNA levels were increased relative to alcohol mice (P = 0.01) (Fig. 8*F*).

Alcohol Differentially Affects Hepatic Expression of Key Metabolic Genes Compared with Skeletal Muscle

Finally, as alcohol is most significantly metabolized in the liver, we assessed whether acute alcohol intoxication led to consistent changes in the hepatic expression of the key metabolic genes altered in the skeletal muscle. Interestingly, acute alcohol intoxication had opposing effects on the expression of genes central to the induction of fat metabolism in the liver as the expression of *Pparα* and *Pparδ/β* was decreased, whereas *CD36* was unchanged in the liver by acute alcohol intoxication (Fig. 9, *A*– *C*). Likewise, the change or lack of change, in expression in hepatic glucose regulatory genes (*Pck1* and *Gck*), was also not consistent with what was observed in muscle (Fig. 9, *D* and *E*). However, the substantial induction of *Pdk4* mRNA in response to acute alcohol intoxication was conserved in both the liver and muscle (Fig. 9*F*). Therefore, alcohol-induced changes in a subset of metabolic genes differ across these two metabolic tissues in the first 24 h after alcohol intoxication.

DISCUSSION

In this study, we show that an acute alcohol binge rapidly increases whole body fat oxidation and suppresses glucose oxidation, an effect that lasts for several days. These changes in whole body metabolism coincided with a rapid change in the molecular signature in the skeletal muscle that was consistent with increased fat oxidation and suppressed carbohydrate oxidation (Fig. 10). Although many of the genes that were rapidly altered in the muscle in response to acute

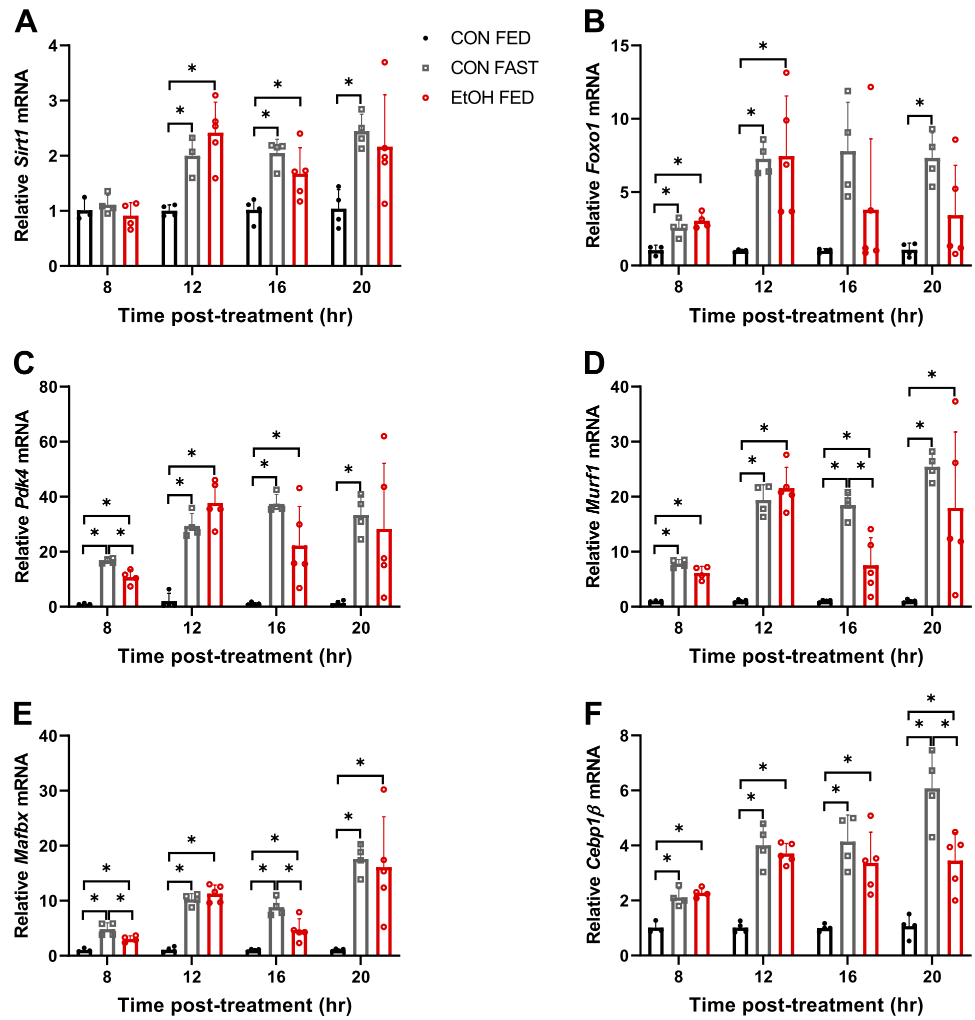

Figure 8. Determination of the potential influence of fasting on alcohol induced changes in skeletal muscle gene expression, including *Sirt1* (*A*), *Foxo1* (*B*), *Pdk4* (*C*), *Murf1* (*D*), *Mafbx* (*E*), and *Cebp1ß* (*F*). The black spheres represent control-fed (CON FED; n = 3–4), the gray open squares control-fasted (CON FAST; n = 4), and the red open spheres alcohol-fed (EtOH FED; n = 4–5). Data are presented as means ± SD for each time point. One-way ANOVA was performed to determine differences between groups at each time point where $P \leq 0.05$. *Significant difference between groups connected by horizontal lines.

alcohol intoxication were putative glucocorticoid target genes, the alcohol-mediated increase in circulating corticosterone levels did not mediate a change in expression of many of those genes indicating alternative mechanisms were contributing. Finally, as many of the fasting-sensitive metabolic targets and metabolites returned to baseline following the clearance of alcohol, alcohol is believed to be inducing distinct effects within the muscle beyond those induced by fasting alone.

The overarching metabolic perturbations caused by acute intoxication included a switch to increased fat metabolism and reduced carbohydrate oxidation (whole body), which coincided with rapid changes in metabolic gene expression specifically within skeletal muscle similar to perturbations induced by fasting. For example, muscle-specific increases in NAD^+/NADH and *Sirt1* mRNA, *Foxo1* and *Cebpβ* mRNA expression, *Pck1* mRNA and PDK4 protein, and promotion of catabolic pathways are all characteristics of the skeletal muscle response to fasting (32–35). In support of the induction of a fasting-like phenotype induced by alcohol intoxication were decreases in blood glucose and increases in free fatty acids and ketones beyond that of fasted animals at 4 and 8 h after intoxication. Upon clearance of alcohol (by 12 h), blood glucose, free fatty acids, and ketones all normalized to control ad libitum fed levels indicating a recovery of metabolic homeostasis. However, despite this recovery of circulating metabolites, normalization of genes sensitive to both alcohol and fasting was slower within the muscle as *Mafbx*, *Cebp1β*, and *Murf1* remained elevated above control-fed levels at the 20-h time point. Overall, acute alcohol intoxication appears to cause a long-lasting energetic stress response in the muscle that mimics the effects of fasting despite normalization of circulating factors that would be indicative of a fasted state (i.e., blood glucose, corticosterone, FFA, ketones) (13). Resolution of these fasting-like effects appears to occur during the second 24 h following intoxication, although variability between subjects and their individual behaviors likely dictates this response.

Skeletal muscle serves as the primary amino acid storage site, whereas amino acid release activated in part by increasing glucocorticoid levels assists in the production of metabolic intermediates including acetyl-CoA and NADPH. Presently, the alcohol-mediated increase in *Bcat2, Idh1*, and *Dbt* mRNA expression may lead to the release of amino acids for production of additional substrate for entry into the TCA cycle. As *Dbt* and *Bcat2* are also increased in alcohol-treated C2C12 myotubes, this is a

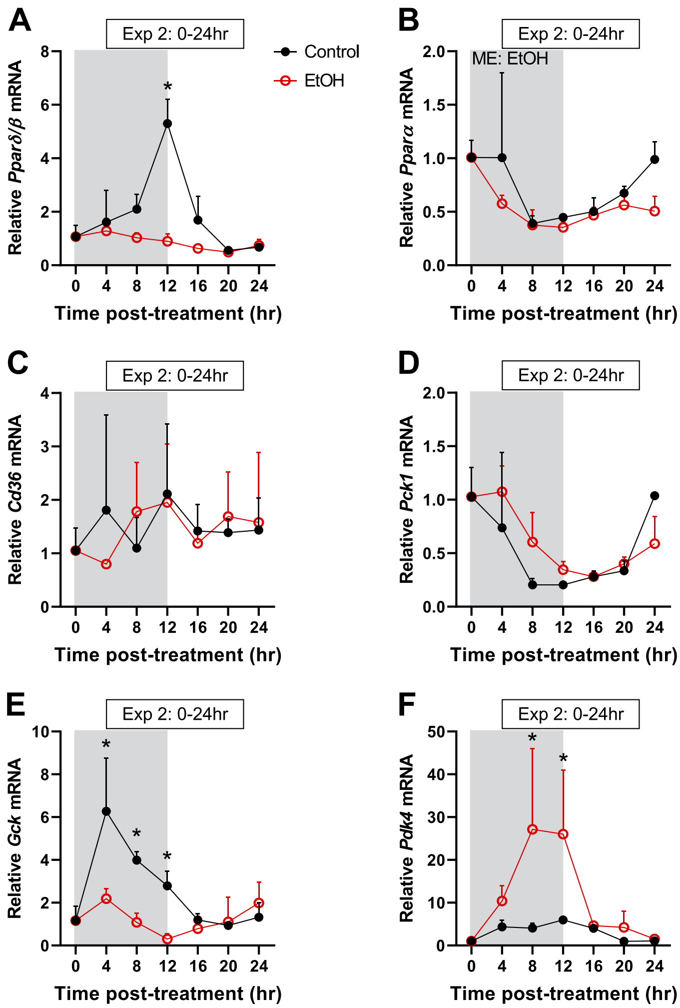

Figure 9. The effects of acute alcohol intoxication on selected metabolic genes within the liver including *Pparδ/β* (*A*), *Pparα* (*B*), *CD36* (*C*), *Pck1* (*D*), *Gck* (*E*), and *Pdk4* (*F*). The gray shading shows the dark cycle (0–12 h, 24–36 h), whereas white boxes indicate the light cycle (12–24 h, 36–48 h). The 0-h time point is the time of injection and baseline tissue collection (n = 3). The black spheres represent control (n = 3), and the open red spheres represent EtOH (n = 3). Data are presented as means ± SD for each time point. Main effects and interactions were determined by two-way ANOVA (Time, EtOH) where $P \leq 0.05$, and the main effect of alcohol is displayed on the graph as ME:EtOH. When there is a significant interaction between Time and EtOH, differences between Control and EtOH are indicated by (*).

muscle-specific and not circulation- or metabolite-dependent effect (36). The components of the branched-chain α-keto acid dehydrogenase (BCKDH) complex, which uses available branched-chain α-keto acids synthesized from branched-chain amino acid catabolism, are regulated by KLF15, PGC1α, PPARs, and CEBPα (37) and accordingly, *Klf15, Pparα,* and *Pparδ/β* were increased at multiple time points throughout the 48-h posttreatment period providing a point of intersection between the regulation of carbohydrate and fat metabolism and resulting amino acid flux. *Klf15, Pparα,* and *Pparδ/β* are also glucocorticoid receptor target genes along with *Murf1, Mafbx,* and *Cebpβ* (31). Although the alcohol-induced increase in *Klf-15, FoxO3a,* and *Murf1* mRNA was mediated by corticosterone, the induction of *Ppar, Cebpβ*, and *Foxo1* mRNA was not. This was unexpected, as CEBPβ is upregulated by exogenous glucocorticoid administration and sensitive to corticosterone inhibition, whereas the FOXO transcription factors are also highly sensitive to glucocorticoid elevations and are under at least partial control of KLF15 (31, 32, 38). Altogether, these findings suggest that glucocorticoids are not the only catalyst of the initial transcriptional and translational changes in metabolic factors induced by acute alcohol intoxication in the skeletal muscle.

Whole body measurements, levels of circulating metabolites, and the skeletal muscle molecular signature support an alcohol-induced enhancement in fat oxidation and suppression of carbohydrate metabolism following intoxication. This includes the enhancement of plasma free fatty acids and β-hydroxybutyrate at 8 h after intoxication which may have had inhibitory effects on glycolysis or glucose uptake and metabolism (39–41). The sustained decrease in carbohydrate oxidation is most evident from the prolonged enhancement in PDK4, whereas genes indicative of β-oxidation were increased by alcohol including *Pparα, Pparδ/β,* and *Cd36* (42). However, how the increase in fat metabolism compared with the decrease in carbohydrate metabolism influenced citric acid cycle activity and thereby NAD+ levels require further investigation. Previous in vitro findings showed that alcohol decreased pyruvate and all TCA cycle intermediates except for succinate in C2C12 myotubes (43), potentially explaining some of the increase in NAD+ presently observed. Furthermore, as alcohol is well known to enhance liver NADH levels, this finding, along with the differing gene expression profiles observed presently in the liver, indicates that despite the metabolic nature of these two tissues, skeletal muscle and liver have divergent responses to binge alcohol intoxication. The capacity to metabolize alcohol may be a contributing factor to this effect as the abundance of alcohol dehydrogenase (ADH) and aldehyde dehydrogenase (ALDH) that generates NADH from NAD+ when converting alcohol to acetate is higher in the liver than skeletal muscle. Therefore, changes in substrate metabolism are tissue-specific and time-specific, despite whole body metabolic effects supporting an increase in fat oxidation and decrease in carbohydrate use.

A few questions remain related to the metabolic effects of acute alcohol intoxication. First, only female mice were used presently despite their lower prevalence of binge drinking, as they are more prone to hangover symptoms and are sensitive to alcoholic disease and related health consequences (20–22, 44, 45). Therefore, it is critical that follow-up experiments also assess the metabolic response to alcohol intoxication in males. In addition, manipulation of alcohol dose, intoxication time and route, as well as number of lifetime binges, will be required to better characterize this response and assess any longer-term implications of this acute metabolic disruption. Finally, whether repeated binge episodes would induce other pathological effects within the muscle, similar to the effects of chronic consumption in the liver, and potentially contribute to future insulin resistance or metabolic dysfunction similar to that observed during chronic alcohol consumption remains to be determined (46).

Overall, these data indicate that an acute alcohol binge leads to significant alterations in skeletal muscle metabolism, including a prolonged shift in lipid oxidation and

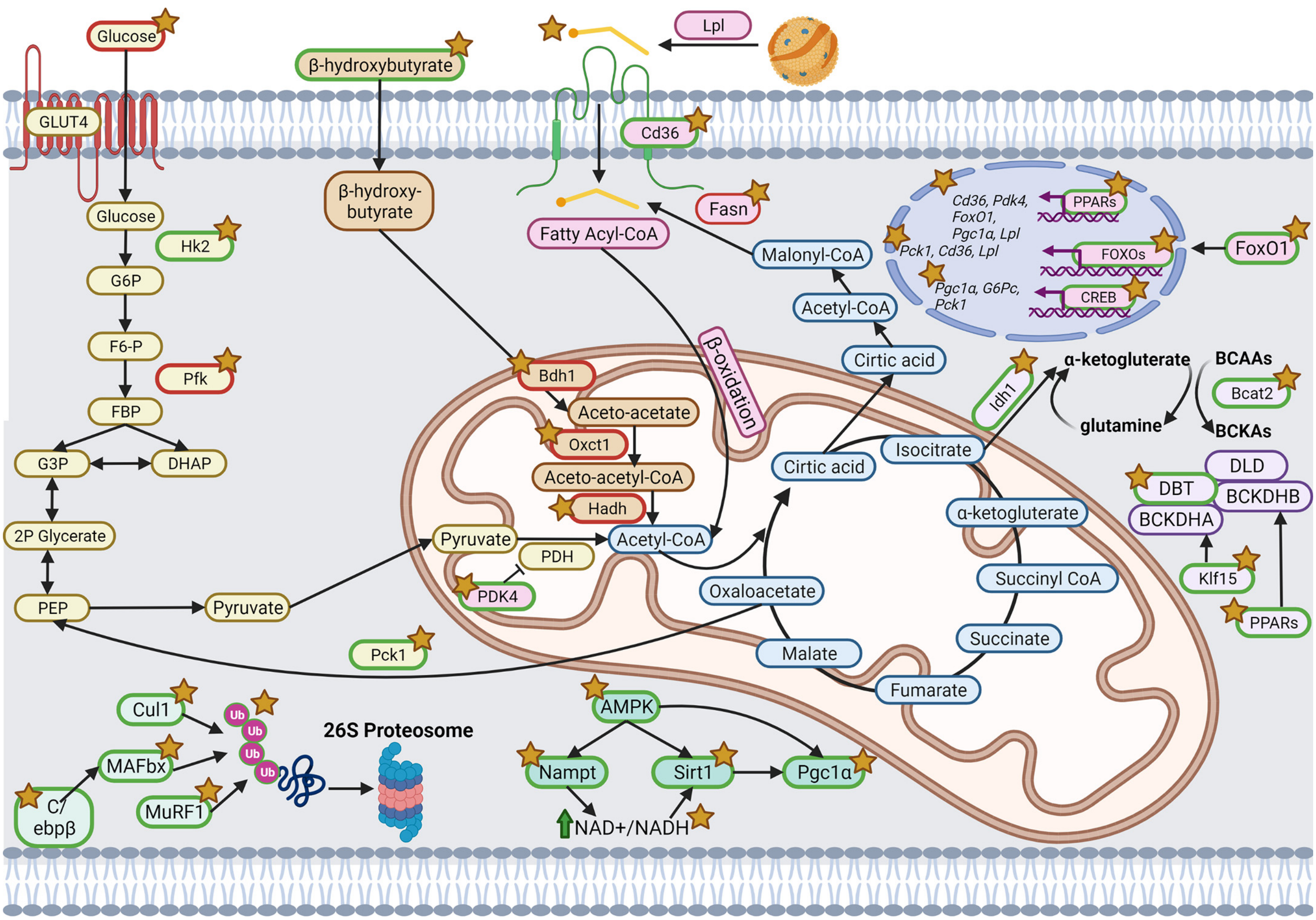

Figure 10. A summary of the metabolic pathways probed in this study. Stars indicate genes and proteins measured in the study, whereas other components of the pathways are provided for context. The green shading indicates genes and proteins within catabolic pathways including AMPK, C/EBPβ, MAFbx, MuRF1, CUL1, as well as ubiquitinated proteins and the proteosome. Purple shading indicates branch chain amino acid degradative pathways components including IDH1, BCAT2, KLF15, PPAR's, PGC1α, branch chain keto acid dehydrogenase E1 subunit α (BCKDHA) and β (BCKDHB), dihydrolipoamide dehydrogenase (DLD), and DBT. The yellow shading represents components of carbohydrate metabolism. This includes the glycolysis pathway components, hexokinase (Hk2), glucose-6 phosphate (G6P), fructose-6 phosphate (F6-P), PFK, fructose 1,6-biphosphate (FBP), phosphoenolpyruvate (PEP), pyruvate and pyruvate dehydrogenase (PDH). Orange shading signifies components of ketone metabolism including plasma and skeletal muscle β-hydroxybutyrate, BDH1, acetoacetate, OXCT1, aceto-acetyl-CoA, and PDK4. Pink shading represents components of lipid metabolism including LPL, CD36, acyl-CoA synthase (ACSL), and fatty-acyl-CoA, FASN. Red outlines indicate repressed expression and green outlines indicate enhanced expression following acute alcohol intoxication. Created with BioRender.com. FASN, fatty acid synthase.

suppression of carbohydrate oxidation. Importantly, humans may also experience a prolonged metabolic dysfunction following a binge drinking episode potentially contributing to impairments in performance, although a definitive link remains to be established (47). Whether differences in dietary intake during recovery from the binge episode would accelerate or further impair skeletal muscle metabolism also remains to be determined as it is conceivable that the intake of higher fat food items may exacerbate or prolong the impairment in skeletal muscle carbohydrate and fat oxidation observed presently (48).

SUPPLEMENTAL DATA

Supplemental Figure S1: https://doi.org/10.6084/m9.figshare.20067590.v1

Supplemental Figure S2: https://doi.org/10.6084/m9.figshare.20067599.v1

Supplemental Figure S3: https://doi.org/10.6084/m9.figshare.20067602.v1

Supplemental Figure S4: https://doi.org/10.6084/m9.figshare.20067623.v1

Supplemental Figure S5: https://doi.org/10.6084/m9.figshare.20067626.v1

GRANTS

The Comprehensive Laboratory Animal Monitoring Systems was provided in part by the FSU Research and Creativity: EIEG program and NIH R01DC013080 to D. A. Fadool. Funding for this work was also provided by Florida State University Start-Up funding to J. L. Steiner and B. S. Gordon.

DISCLOSURES

No conflicts of interest, financial or otherwise, are declared by the authors.

AUTHOR CONTRIBUTIONS

A.L.T. and J.L.S. conceived and designed research; A.L.T., J.A.L., B.S.G., and J.L.S. performed experiments; A.L.T., J.A.L., and J.L.S. analyzed data; A.L.T., J.A.L., D.A.F., B.S.G., and J.L.S. interpreted results of experiments; A.L.T. and J.L.S. prepared figures; A.L.T. and J.L.S. drafted manuscript; A.L.T., J.A.L., D.A.F., B.S.G., and J.L.S. edited and revised manuscript; A.L.T., J.A.L., D.A.F., B.S.G., and J.L.S. approved final version of manuscript.

REFERENCES

1. **Kanny D**, **Naimi TS**, **Liu Y**, **Lu H**, **Brewer RD.** Annual total binge drinks consumed by U.S. adults, 2015. *Am J Prev Med* 54: 486–496, 2018. doi:10.1016/j.amepre.2017.12.021.
2. **Dasarathy J**, **McCullough AJ**, **Dasarathy S.** Sarcopenia in alcoholic liver disease: clinical and molecular advances. *Alcohol Clin Exp Res* 41: 1419–1431, 2017. doi:10.1111/acer.13425.
3. **Esser MB**, **Hedden SL**, **Kanny D**, **Brewer RD**, **Gfroerer JC**, **Naimi TS.** Prevalence of alcohol dependence among US adult drinkers, 2009-2011. *Prev Chronic Dis* 11: E206, 2014. doi:10.5888/pcd11.140329.
4. **Steiner JL**, **Lang CH.** Dysregulation of skeletal muscle protein metabolism by alcohol. *Am J Physiol Endocrinol Metab* 308: E699–E712, 2015. doi:10.1152/ajpendo.00006.2015.
5. **Wolfe RR.** The underappreciated role of muscle in health and disease. *Am J Clin Nutr* 84: 475–482, 2006. doi:10.1093/ajcn/84.3.475.
6. **Meyer C**, **Dostou JM**, **Welle SL**, **Gerich JE.** Role of human liver, kidney, and skeletal muscle in postprandial glucose homeostasis. *Am J Physiol Endocrinol Metab* 282: E419–E427, 2002. doi:10.1152/ajpendo.00032.2001.
7. **Argilés JM**, **Campos N**, **Lopez-Pedrosa JM**, **Rueda R**, **Rodriguez-Mañas L.** Skeletal muscle regulates metabolism via interorgan crosstalk: roles in health and disease. *J Am Med Dir Assoc* 17: 789–796, 2016. doi:10.1016/j.jamda.2016.04.019.
8. **Rasmussen BB**, **Wolfe RR.** Regulation of fatty acid oxidation in skeletal muscle. *Annu Rev Nutr* 19: 463–484, 1999. doi:10.1146/annurev.nutr.19.1.463.
9. **Rochlani Y**, **Pothineni NV**, **Kovelamudi S**, **Mehta JL.** Metabolic syndrome: pathophysiology, management, and modulation by natural compounds. *Ther Adv Cardiovasc Dis* 11: 215–225, 2017. p doi:10.1177/1753944717711379.
10. **Spolarics Z**, **Bagby GJ**, **Pekala PH**, **Dobrescu C**, **Skrepnik N**, **Spitzer JJ.** Acute alcohol administration attenuates insulin-mediated glucose use by skeletal muscle. *Am J Physiol Endocrinol Physiol* 267: E886–E891, 1994. doi:10.1152/ajpendo.1994.267.6.E886.
11. **Suter PM**, **Gerritsen-Zehnder M**, **Häsler E**, **Gürtler M**, **Vetter W**, **Hänseler E.** Effect of alcohol on postprandial lipemia with and without preprandial exercise. *J Am Coll Nutr* 20: 58–64, 2001. doi:10.1080/07315724.2001.10719015.
12. **McGuire LC**, **Cruickshank AM**, **Munro PT.** Alcoholic ketoacidosis. *Emerg Med J* 23: 417–420, 2006. doi:10.1136/emj.2004.017590.
13. **Tice AL**, **Laudato JA**, **Rossetti ML**, **Wolff CA**, **Esser KA**, **Lee C**, **Lang CH**, **Vied C**, **Gordon BS**, **Steiner JL.** Binge alcohol disrupts skeletal muscle core molecular clock independent of glucocorticoids. *Am J Physiol Endocrinol Metab* 321: E606–E620, 2021. doi:10.1152/ajpendo.00187.2021.
14. **Kuo T**, **Harris CA**, **Wang JC.** Metabolic functions of glucocorticoid receptor in skeletal muscle. *Mol Cell Endocrinol* 380: 79–88, 2013. doi:10.1016/j.mce.2013.03.003.
15. **Britto FA**, **Begue G**, **Rossano B**, **Docquier A**, **Vernus B**, **Sar C**, **Ferry A**, **Bonnieu A**, **Ollendorff V**, **Favier FB.** REDD1 deletion prevents dexamethasone-induced skeletal muscle atrophy. *Am J Physiol Endocrinol Metab* 307: E983–E993, 2014. doi:10.1152/ajpendo.00234.2014.
16. **Qi D**, **An D**, **Kewalramani G**, **Qi Y**, **Pulinilkunnil T**, **Abrahani A**, **Al-Atar U**, **Ghosh S**, **Wambolt RB**, **Allard MF**, **Innis SM**, **Rodrigues B.** Altered cardiac fatty acid composition and utilization following dexamethasone-induced insulin resistance. *Am J Physiol Endocrinol Metab* 291: E420–E427, 2006. doi:10.1152/ajpendo.00083.2006.
17. **Puthanveetil P**, **Wang F**, **Kewalramani G**, **Kim MS**, **Hosseini-Beheshti E**, **Ng N**, **Lau W**, **Pulinilkunnil T**, **Allard M**, **Abrahani A**, **Rodrigues B.** *Cardiac glycogen accumulation after dexamethasone is regulated by AMPK. Am J Physiol Heart Circ Physiol* 295: H1753–H1762, 2008. doi:10.1152/ajpheart.518.2008.
18. **Laudato JA**, **Tice AL**, **Call JA**, **Gordon BS**, **Steiner JL.** Effects of alcohol on skeletal muscle contractile performance in male and female mice. *PLoS One* 16: e0255946, 2021. doi:10.1371/journal.pone.0255946.
19. **Alford C**, **Broom C**, **Carver H**, **Johnson SJ**, **Lands S**, **Reece R**, **Verster JC.** The impact of alcohol hangover on simulated driving performance during a 'commute to work'-zero and residual alcohol effects compared. *J Clin Med* 9: 1435, 2020. doi:10.3390/jcm9051435.
20. **Becker U**, **Deis A**, **Sørensen TI**, **Grønbaek M**, **Borch-Johnsen K**, **Müller CF**, **Schnohr P**, **Jensen G.** Prediction of risk of liver disease by alcohol intake, sex, and age: a prospective population study. *Hepatology* 23: 1025–1029, 1996. doi:10.1002/hep.510230513.
21. **Fulham MA**, **Mandrekar P.** Sexual dimorphism in alcohol induced adipose inflammation relates to liver injury. *PLoS One* 11: e0164225, 2016. doi:10.1371/journal.pone.0164225.
22. **Sato N**, **Lindros KO**, **Baraona E**, **Ikejima K**, **Mezey E**, **Järveläinen HA**, **Ramchandani VA.** Sex difference in alcohol-related organ injury. *Alcohol Clin Exp Res* 25: 40S–45S, 2001. doi:10.1111/j.1530-0277.2001.tb02371.x.
23. **Bell GA**, **Fadool DA.** Awake, long-term intranasal insulin treatment does not affect object memory, odor discrimination, or reversal learning in mice. *Physiol Behav* 174: 104–113, 2017. doi:10.1016/j.physbeh.2017.02.044.
24. **van Loon LJ**, **Greenhaff PL**, **Constantin-Teodosiu D**, **Saris WH**, **Wagenmakers AJ.** The effects of increasing exercise intensity on muscle fuel utilisation in humans. *J Physiol* 536: 295–304, 2001. doi:10.1111/j.1469-7793.2001.00295.x.
25. **Jacobi D**, **Liu S**, **Burkewitz K**, **Kory N**, **Knudsen NH**, **Alexander RK**, **Unluturk U**, **Li X**, **Kong X**, **Hyde AL**, **Gangl MR**, **Mair WB**, **Lee C-H.** Hepatic Bmal1 regulates rhythmic mitochondrial dynamics and promotes metabolic fitness. *Cell Metab* 22: 709–720, 2015. doi:10.1016/j.cmet.2015.08.006.
26. **Rossetti ML**, **Esser KA**, **Lee C**, **Tomko RJ**, **Eroshkin AM**, **Gordon BS.** Disruptions to the limb muscle core molecular clock coincide with changes in mitochondrial quality control following androgen depletion. *Am J Physiol Endocrinol Metab* 317: E631–E645, 2019. doi:10.1152/ajpendo.00177.2019.
27. **Li L**, **Li T**, **Zhang Y**, **Pan Z**, **Wu B**, **Huang X**, **Zhang Y**, **Mei Y**, **Ge L**, **Shen G**, **Ge R-S**, **Zhu D**, **Lou Y.** Peroxisome proliferator-activated receptorβ/δ activation is essential for modulating p-Foxo1/Foxo1 status in functional insulin-positive cell differentiation. *Cell Death Dis* 6: e1715, 2015. doi:10.1038/cddis.2015.88.
28. **Gross DN**, **Wan M**, **Birnbaum MJ.** The role of FOXO in the regulation of metabolism. *Curr Diab Rep* 9: 208–214, 2009. doi:10.1007/s11892-009-0034-5.
29. **Ehrenborg E**, **Krook A.** Regulation of skeletal muscle physiology and metabolism by peroxisome proliferator-activated receptor delta. *Pharmacol Rev* 61: 373–393, 2009. doi:10.1124/pr.109.001560.
30. **Burri L**, **Thoresen GH**, **Berge RK.** The role of PPARα activation in liver and muscle. *PPAR Res*, 2010: 1–11, 2010. doi:10.1155/2010/542359.
31. **Braun TP**, **Marks DL.** The regulation of muscle mass by endogenous glucocorticoids. *Front Physiol* 6: 12, 2015. doi:10.3389/fphys.2015.00012.
32. **Allen DL**, **Cleary AS**, **Hanson AM**, **Lindsay SF**, **Reed JM.** CCAAT/enhancer binding protein-delta expression is increased in fast skeletal muscle by food deprivation and regulates myostatin transcription in vitro. *Am J Physiol Regul Integr Comp Physiol* 299: R1592–R1601, 2010. doi:10.1152/ajpregu.00247.2010.
33. **Millet L**, **Vidal H**, **Andreelli F**, **Larrouy D**, **Riou JP**, **Ricquier D**, **Laville M**, **Langin D.** Increased uncoupling protein-2 and -3 mRNA expression during fasting in obese and lean humans. *J Clin Invest* 100: 2665–2670, 1997. doi:10.1172/JCI119811.
34. **Lopez-Soldado I**, **Guinovart JJ**, **Duran J.** Increased liver glycogen levels enhance exercise capacity in mice. *J Biol Chem* 297: 100976, 2021. doi:10.1016/j.jbc.2021.100976.
35. **Ogata T**, **Oishi Y**, **Higuchi M**, **Muraoka I.** Fasting-related autophagic response in slow- and fast-twitch skeletal muscle. *Biochem Biophys Res Commun* 394: 136–140, 2010. doi:10.1016/j.bbrc.2010.02.130.
36. **Singh SS**, **Kumar A**, **Welch N**, **Sekar J**, **Mishra S**, **Bellar A**, **Gangadhariah M**, **Attaway A**, **Al Khafaji H**, **Wu X**, **Pathak V**,

Agrawal V, **McMullen MR**, **Hornberger TA**, **Nagy LE**, **Davuluri G**, **Dasarathy S.** Multiomics-identified intervention to restore ethanol-induced dysregulated proteostasis and secondary sarcopenia in alcoholic liver disease. *Cell Physiol Biochem* 55: 91–116, 2021. doi:10.33594/000000327.

37. **Biswas D**, **Duffley L**, **Pulinilkunnil T.** Role of branched-chain amino acid-catabolizing enzymes in intertissue signaling, metabolic remodeling, and energy homeostasis. *FASEB J* 33: 8711–8731, 2019. doi:10.1096/fj.201802842RR.
38. **Yang H**, **Mammen J**, **Wei W**, **Menconi M**, **Evenson A**, **Fareed M**, **Petkova V**, **Hasselgren P-O.** Expression and activity of C/EBPβ and Δ are upregulated by dexamethasone in skeletal muscle. *J Cell Physiol* 204: 219–226, 2005. doi:10.1002/jcp.20278.
39. **Yamada T**, **Zhang S-J**, **Westerblad H**, **Katz A.** {β}-Hydroxybutyrate inhibits insulin-mediated glucose transport in mouse oxidative muscle. *Am J Physiol Endocrinol Metab* 299: E364–E373, 2010. doi:10.1152/ajpendo.00142.2010.
40. **Garland PB**, **Newsholme EA**, **Randle PJ.** Regulation of glucose uptake by muscle 9. Effects of fatty acids and ketone bodies, and of alloxan-diabetes and starvation, on pyruvate metabolism and on lactate-pyruvate and L-glycerol 3-phosphate-dihydroxyacetone phosphate concentration ratios in rat heart and rat diaphragm muscles. *Biochem J* 93: 665–678, 1964. doi:10.1042/bj0930665.
41. **Newsholme EA.** Carbohydrate metabolism in vivo: regulation of the blood glucose level. *Clin Endocrinol Metab* 5: 543–578, 1976. doi:10.1016/S0300-595X(76)80040-0.
42. **Manickam R**, **Wahli W.** Roles of peroxisome proliferator-activated receptor β/Δ in skeletal muscle physiology. *Biochimie* 136: 42–48, 2017. doi:10.1016/j.biochi.2016.11.010.
43. **Kumar A**, **Davuluri G**, **Welch N**, **Kim A**, **Gangadhariah M**, **Allawy A**, **Priyadarshini A**, **McMullen MR**, **Sandlers Y**, **Willard B**, **Hoppel CL**, **Nagy LE**, **Dasarathy S.** Oxidative stress mediates ethanol-induced skeletal muscle mitochondrial dysfunction and dysregulated protein synthesis and autophagy. *Free Radic Biol Med* 145: 284–299, 2019. doi:10.1016/j.freeradbiomed.2019.09.031.
44. **Vatsalya V**, **Stangl BL**, **Schmidt VY**, **Ramchandani VA.** Characterization of hangover following intravenous alcohol exposure in social drinkers: methodological and clinical implications. *Addict Biol* 23: 493–502, 2018. doi:10.1111/adb.12469.
45. **Wilsnack RW**, **Wilsnack SC**, **Gmel G**, **Kantor LW.** Gender differences in binge drinking: prevalence, predictors, and consequences. *Alcohol Res* 39: 57–76, 2018.
46. **Kelley DE**, **Goodpaster BH**, **Storlien L.** Muscle triglyceride and insulin resistance. *Annu Rev Nutr* 22: 325–346, 2002. doi:10.1146/annurev.nutr.22.010402.102912.
47. **Barnes MJ**, **Mundel T**, **Stannard SR.** Acute alcohol consumption aggravates the decline in muscle performance following strenuous eccentric exercise. *J Sci Med Sport* 13: 189–193, 2010. doi:10.1016/j.jsams.2008.12.627.
48. **Morley KC**, **Logge WB**, **Riordan BC**, **Brannon S**, **Haber PS**, **Conner TS.** Daily experiences of hangover severity and food consumption in young adults. *Br J Health Psychol* 27: 468–483, 2022. doi:10.1111/bjhp.12555.